Carbazole-Based Electroluminescent Devices Obtained by Vacuum Evaporation

K. D'ALMEIDA,[1] J. C. BERNÈDE,[1] F. RAGOT,[2] A. GODOY,[3] F. R. DIAZ,[3] S. LEFRANT[2]

[1] EPSE, FSTN, BP 92208, Fr.44322, Nantes cedex 3, France

[2] LPC-IMJR, BP 92208, Fr.44322, Nantes cedex 3, France

[3] Faculty of Chemistry, PUCC, P.O. Box, Santiago 22, Chile

Received 19 December 2000; accepted 21 February 2001

ABSTRACT: Transparent conductive oxide (SnO_2)/organic layers/aluminum thin film sandwich structures were obtained by vacuum evaporation. The organic component was either a thin carbazole film or a bilayer. In that case, the carbazole film was deposited onto a thin insulating polymer film. The polymer used was the poly(tetrabromo-*p*-phenyleneselenide) (PBrPDSe). Photoluminescence measurements have shown that the carbazole thin films emit blue light. (*I-V*) measurements have shown that the structures exhibit diode characteristics. The forward direction is obtained when the transparent conductive oxide (TCO) is positively biased. However, the reproducibility of the results obtained with a single carbazole layer is poor. It appears that the stability of the sample is improved when a thin PBrPDSe film (40 nm) is introduced between the carbazole and the SnO_2. The polymer film avoids the short circuit effect. In that case, the turn-on voltage of the diode is about 3 V, when the thickness of the carbazole film is around 250 nm and the electroluminescence appears at a voltage of about 5 V. It is shown that the thermionic effect cannot be used to explain the *I-V* characteristics, which are interpreted with the help of the Fowler–Nordheim tunnel effect. © 2001 John Wiley & Sons, Inc. J Appl Polym Sci 82: 2042–2055, 2001

Key words: organic light emitting diodes; evaporated thin films; carbazole; poly(tetrabromo-*p*-phenyleneselenide); luminescence

INTRODUCTION

Since the electroluminescence of the film poly(1.4-phenylene vinylene) (PPV)-based diodes was reported by Burroughes and colleagues[1] in 1990, organic electroluminescence (EL) has been the subject of increasing worldwide interest.

Such organic electroluminescent diodes (OLED) are very promising for commercial display devices, signs, and lighting.[2]

The carbazole family (Scheme 1) forms a subset of the organic materials under study for blue EL applications. Polyvinycarbazole,[3–5] polycarbazole,[6] and many others derivatives[7–12] were used to achieve blue OLED.

Problems do, however, still exist and before commercial applications can be realized, further work needs to be undertaken concerning the issues of long-term stability, emission efficiency, device addressing schemas, and others.

Correspondence to: J. C. Bernède.

Contract grant sponsor: ECOS-CONICYT; Contract grant number: 99-E05.

Journal of Applied Polymer Science, Vol. 82, 2042–2055 (2001)

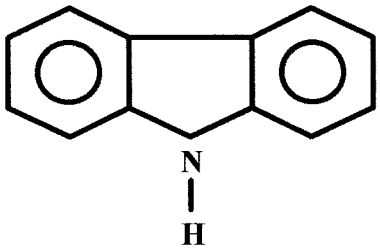

Scheme 1

Usually thin films are prepared from organic material in solution by spin coating onto transparent conductive oxide (TCO)-coated glasses. Although excellent results were achieved this way, there are a number of problems that can arise. It could be difficult to find suitable solvents to prepare thin films (50–400 nm) that are free from pinholes.

Mutually exclusive solvents for the different polymer layers in a multilayer device are difficult to engineer.

Oxygen and other contaminants (e.g., dust) are difficult to exclude from the solutions used and therefore from the films.

Solvent not fully removed from the films after deposition can cause formation of voids and chemical reactivity with the electrodes.

An alternative approach that can avoid such difficulties is vacuum evaporation. Vapor deposition under vacuum provides a clean environment; it is solvent free and is well suited to sequential depositions. Moreover, the device fabrications use vacuum deposition of the metal upper electrode, which allows a whole processing in the same run.

Vapor deposition was often used for sublimation of low-molecular-weight dyes, [13] oligomers,[14–15] and polymers.[16–18]

The evaporated organic bilayer structure tris (8-hydroxyquinoline aluminum) (Alq_3), poly(*N*-vinyl-carbazole) (PVK) was already realized.[19]

However, we have shown[20] that PVK evaporation induces a shortening effect of the polymer chain length. The deposited film is composed of oligomers with a broad distribution of the chain length.

In this study, we choose, for simplicity, to work with carbazole (CZ). Our purpose consists of developing a simple route to obtain reproducible devices for the study of the interface TCO anode/organic film. Two sample families were used for such purposes: SnO_2/CZ/Al and SnO_2/PBrPDSe/CZ/Al, where PBrPDSe, the poly(tetrabromo-*p*-phenyleneselenide), is a thin, very insulating and homogeneous film.

SAMPLE PREPARATION

The TCO used was commercial SnO_2 (Solems). The whole glass substrate was covered; therefore, some SnO_2 must be removed. After masking a broad line of 2 mm, the SnO_2 was etched by using Zn + HCl as etchant.[21]

Then the substrates were cleaned by using the H_2O_2 treatment following a process described by Osada and colleagues,[22] which corresponds to the first solution (SC1) of the RCA process first described by Kern and Puotinen.[23] The substrates were treated with an 80°C H_2O—H_2O_2 (30%)—NH_4OH (25%) solution (5 : 1 : 1 vol parts) for 20 min, followed by rinsing with boiling distilled H_2O for 5 min. The use of boiling water was proven to be helpful to obtain impurity-free surfaces.[24]

The organic compounds used were PBrPDSe and CZ. The PBrPDSe powder was obtained according to the reaction shown below, which was described in a preceding article[25] (Scheme 2).

Because the evaporation route was elected to achieve the whole device, it was necessary to use monomer (CZ) and/or stable polymer to avoid decomposition during the joule heating necessary for the sublimation under vacuum. It was shown[26] that polymers with substituted halogen are more stable. Therefore, because some authors of the present work dominated the synthesis of PBrPDSe, it was used as the second organic layer in the diodes presently tested.

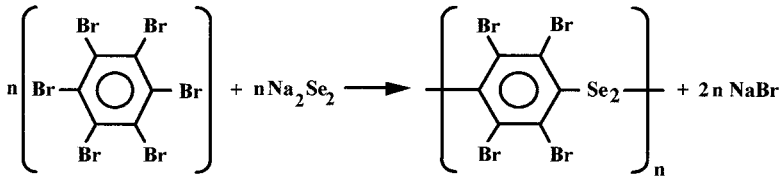

Scheme 2

The depositing apparatus was equipped with a Pyrex glass chamber designed in the laboratory. The substrate holder was cooled by melting ice. The thickness of the organic layers were measured *in situ* by an h.f. quartz monitor. The thicknesses were checked by cross section visualization by using a scanning electron microscope (SEM). All the depositions were done in a vacuum of 10^{-3} Pa.

The PBrPDSe and the carbazole films were deposited from laboratory-made cells. To avoid strong decomposition of the polymer by overheating during the deposition process, the evaporation cell temperature was measured by a copper-constantan thermocouple introduced into the Pyrex cell. The deposition rates, v, were 0.5 and 2 nm s^{-1} for PBrPDSe and CZ, respectively.

Finally, Al contacts were deposited onto the organic layers by vacuum evaporation at low pressure close to 10^{-4} Pa. A mask was used to determine a well-defined shape for the Al electrodes, which gives an active area of 4 mm^2. During Al deposition, the substrate holder was cooled by liquid nitrogen to minimize organic film degradation and Al diffusion.

Two different types of device structures were fabricated. In each case, SnO_2 was used as the anode and Al as the cathode. The device types were as follows: Device 1: SnO_2/carbazole/Al carbazole thickness 100–600 nm

Device 2: SnO_2/PBrPDSe/carbazole/Al PBrPDSe thickness 50 nm, and CZ, the same thickness range as device 1 (i.e., $100 \leq t \leq 600$ nm)

CHARACTERIZATION TECHNIQUES

To check the quality of the films, the films were studied by infrared absorption measurement (*I-R*), SEM, and photoluminescent measurements. The devices were studied by current-voltage (*I-V*) and electroluminescence-voltage (*EL-V*) measurements. Also, some X-ray photoelectron spectroscopy (XPS) depth profiles were done on typical samples.

Infrared spectra were obtained with an FTIR spectrometer. Absorption band positions are given in wave numbers (cm^{-1}).

Observation of the morphology of the surface and of the cross section of the layers were performed by using a Jeol 6400F field-effect SEM to compare the surface topography of the PBrPDSe and the CZ and to check the cross section.

The photoluminescence (PL) spectra were recorded using the Jobin–Yvon TG HG2S spectrophotometer with holographic gratings. The signal was detected with a Peltier-cooled photomultiplier. The sample was excited with the 337-nm line of a filtered xenon lamp (150 W). The light power at the sample was kept below 2 mW. Experiments were performed at room temperature.

For *I-V* and *EL* measurements, sandwich structures SnO_2/PCZ/Al were grown by vacuum evaporation of the aluminum upper electrode. The active area of the OLED was 4 mm^2.

Electron spectroscopy for chemical analysis (ESCA) measurements were conducted with a Leybold spectrometer at the University of Nantes, CNRS. The ESCA was used for XPS measurements. The X-ray source was a magnesium cathode (1253.6 eV) operating at 10 kV and 10 mA. The energy resolution was 1 eV at a pass energy of 50 eV. High-resolution scans with a good signal/noise ratio were obtained in the C1s, Br3d, Se3d, N1s, O1s regions of the spectrum. The quantitative studies were based on the determination of the C1s, Br3d, Se3d, N1s, O1s peak areas with, respectively, 0.2, 0.67, 0.57, 0.36, and 0.6 as sensitive factors; the sensitivity factors are given by the manufacturer. The depth profile was obtained by recording successive XPS spectra of the different regions after ion etching for short periods. By using an ion gun, sputtering was accomplished at pressures of less than 5×10^{-4} Pa with a 10-mA emission current and 3-kV beam energy.

EXPERIMENTAL RESULTS

Before diodes characterization, the organic thin films were characterized by different physicochemical techniques.

Thin-Film Characterization

PBrPDSe Thin Films

The thermal gravimetric analysis (TGA) curve of PBrPDSe has shown[27] that the polymer decomposition begins when $T \geq 250$°C. Therefore, during deposition, the evaporation cell was heated at 150°C to prevent polymer decomposition.

The systematical characterization of the films was done earlier.[28] We have shown that the PBrPDSe molecules are not destroyed during the deposition process; however, it appears that the

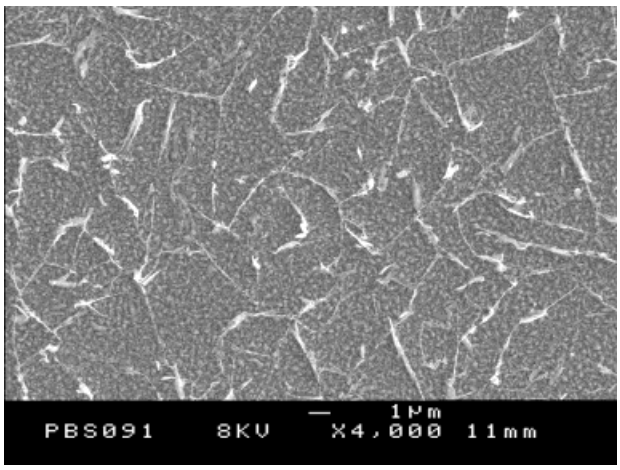

Figure 1 Micrograph of a PBrPDSe thin film, thickness 50 nm.

chain length is strongly reduced. Therefore, the films are composed of oligomers with a broad chain-length distribution.

In the diode structures studied in the present work, the thickness of the PBrPDSe was systematically 50 nm. These thin films were deposited onto a SnO_2-coated glass substrate. Figure 1 shows that the films are composed of a thin homogeneous underlayer from which some randomly distributed heaps appear. It was checked by X-ray diffraction (XRD) that the films are nearly amorphous. The high-coverage efficiency of the PBrPDSe thin film was checked by XPS measurements. When a 50-nm-thick film deposited on SnO_2 is studied by XPS, not only is the tin signal not visible at the surface of the structure but also it is not visible after 5 min of etching, which means that the PBrPDSe thin film covers all the SnO_2 underlayer without any pinholes.

Carbazole Thin Films

The carbazole films deposited by evaporation of carbazole monomer powder have a thickness of 100–600 nm. It was checked by XRD measurements that the structure of the carbazole molecule is not destroyed during the heating for evaporation. Figure 2 presented the diffractograms of a thin film and the reference powder. It can be seen that all the peaks of the powder are visible in the thin-film diagram. It appears that the relative peak intensities are not that of JCPDS 32-1556 (International Center for Diffraction Data–Powder Diffraction Files-2 data base), which attests that there is some grain orientation with a preferential orientation along the (020) direction.

The films were also characterized by XPS. The quantitative analysis is in good agreement with theoretical composition. An amount of 7.7 at. % nitrogen is expected and 6 at. % is measured; moreover, it should be taken into account that there is a small surface contamination by oxygen (3 at. %). Therefore, it can be said that in the error range of the measurement technique, the films are stoichiometric. The oxygen contamination is negligible, because it corresponds to surface contamination related to air exposure of the samples before XPS analysis; often such contamination is more than 3 at. %, which means that, in the present case, there is no strong interaction between the polymer and oxygen. This fact is corroborated by the decomposition of the carbon peak. Only two contributions are required to obtain a good fit between the experimental and the theoretical curves [Fig. 3(a)]. The first contribution situated at 285 eV can be attributed to C—C bonds, whereas the other one, situated at 286 eV, can be attributed to C—N bonds.[29] There is no carbon–oxygen contribution. The N1s peak [Fig. 3(b)] can be simulated by one contribution alone corresponding to the nitrogen bonded to carbon. However, a visualization by SEM shows that the films are highly inhomogeneous. In Figure 4, we reported the same sample surface area using two different SEM modes. In the secondary electron mode, it can be seen that above a more or less homogeneous underlayer, some features with filamentary-like shape are visible [Fig. 4(a)]. If the same region is visualized by the retrodiffusion mode, some areas appear very clear [Fig. 4(b)]. Because the retrodiffusion efficiency increases with the atomic mass of the atoms, the clear domains correspond to heavier atoms (i.e., the film being a polymer) to bare substrate ($SiO_2 \cdots$). Therefore, there is a minimum thickness necessary to obtain pinhole-free layers. Moreover, even when the whole surface of the substrate is covered, the thickness of the film is very inhomogeneous (Fig. 5).

To complete the CZ film characterization, we proceeded to optical measurements. In Figure 6 are reported the transmission spectra of the different samples dissolved in THF. It can be seen that the same bands are present in the two sample families.

The concentration of the two samples being very different, the relative intensities of the peaks are difficult to discuss but their wavelengths are

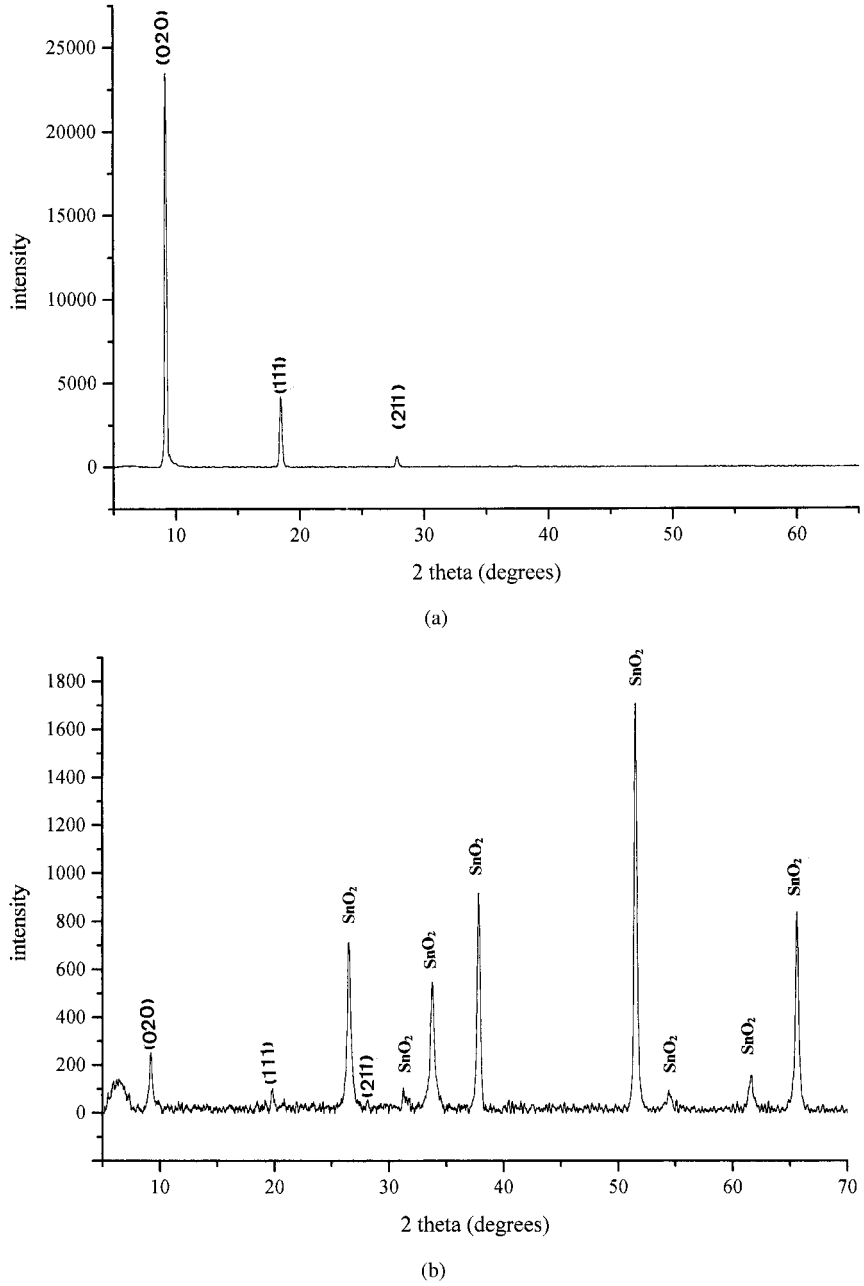

Figure 2 XRD diagram of (a) carbazole powder; (b) carbazole thin film on tin oxide-coated substrate.

identical. As it can be seen in Figure 6, the thin film spectrum has a better resolution than that of the powder. This fact and the varying peak intensities can be explained by a saturation effect in the powder solution.

The photoluminescence curves of the CZ and PBrPDSe reference powders are reported in Figure 7. It can be seen that all the samples emit blue light. The emission intensity of CZ is far higher than that of PBrPDSe and no signal was detected in the case of PBrPDSe thin films, whereas the signal of CZ thin films is similar to that of the powder but with poor resolution. The CZ spectrum is clearly resolved only in the case of powder; it emits blue light with a spectral maximum at 420 nm, secondary peaks at 450 and 400 nm, and shoulders at 470, 490, and 630 nm. The three main peaks (400, 420, 450 nm) can be assigned to 0–0, 0–1, and 0–2 transitions, respec-

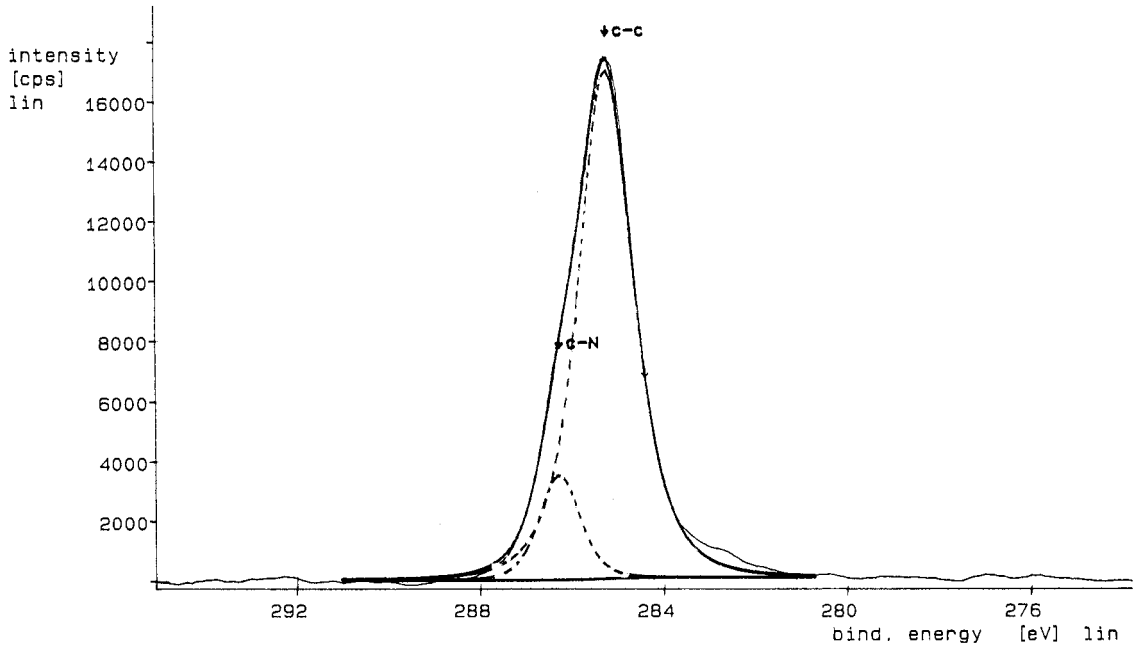

(a)

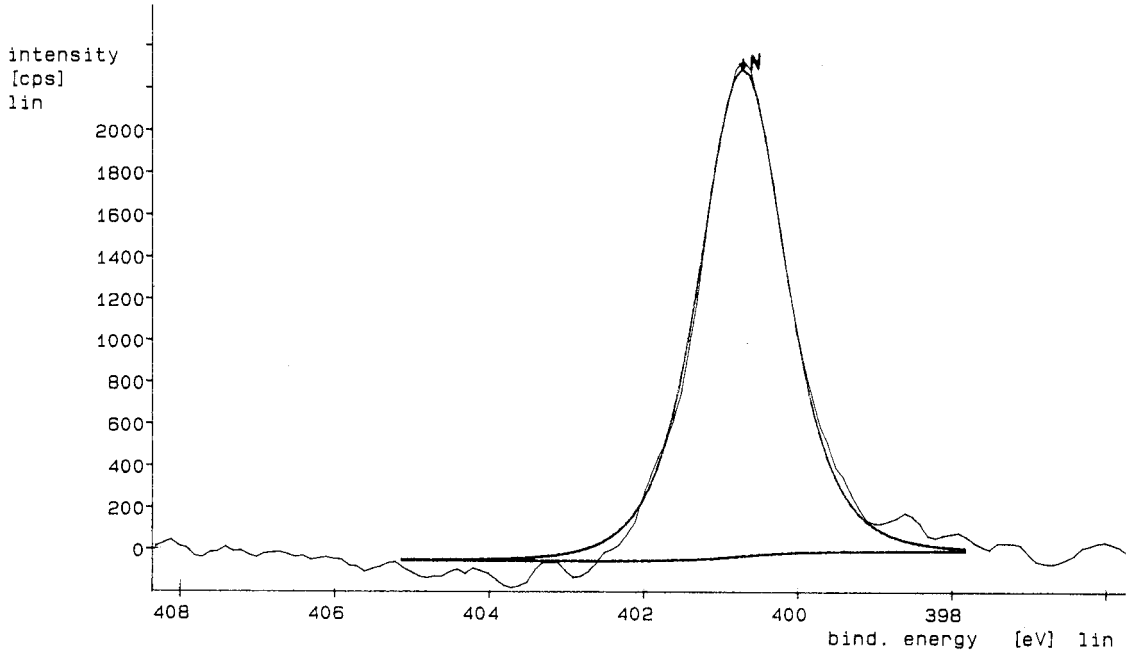

(b)

Figure 3 XPS spectra of a carbazole thin film: (∧-∧) experimental curves; (—) theoretical curves; (- - -) different curves. (a) C1s; (b) N1s.

tively; the shoulders correspond to vibronic side bands.[30]

It can be seen that the light emission of PBrPDSe is centered around 450 nm. After characterization, these films were used for OLED achievement.

Diode Structures Characterization

Experimental Results

For (*I-V*) and (*EL-V*) studies, forward bias is defined with the SnO_2 electrode being wired as the anode. For each diode type, more than 10 samples

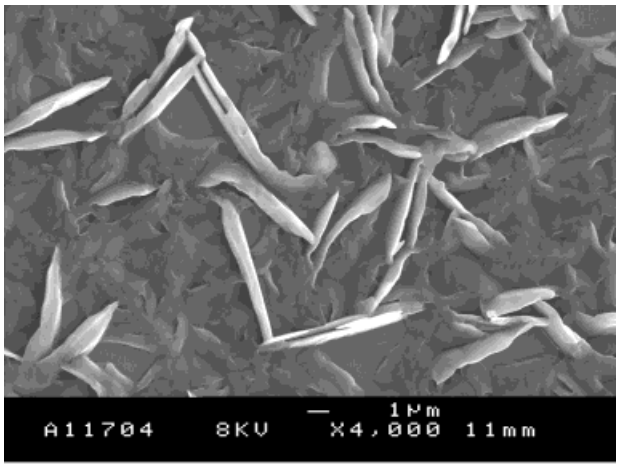

(a)

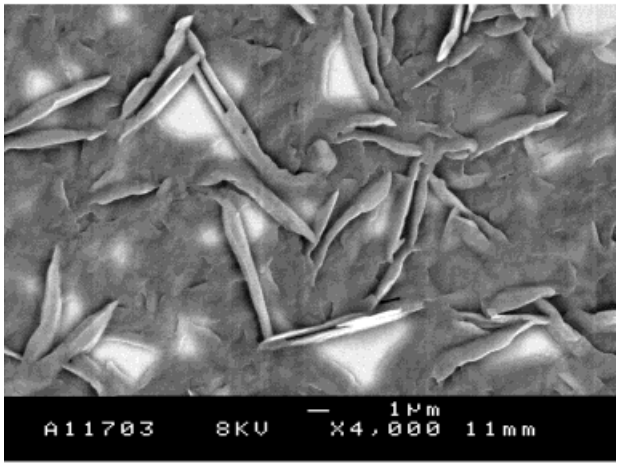

(b)

Figure 4 Micrograph of a CZ film. (a) Secondary electron image; (b) Retrodiffused image.

were characterized. *EL* was measured by using a calibrated photodiode. (*I-V*) and (*EL-V*) characteristics of typical samples are depicted in Figure 8. Single-layer SnO_2/CZ/Al diodes were unstable during the measurement because of leakage currents. SnO_2/PBrPDSe/CZ/Al double-layer diodes were more stable. The OLED turn-on voltages are reported in Table I. It can be seen that it has erratic values in the case of single-layer samples, whereas it increases progressively with the carbazole thickness in the case of double layers, except when the CZ films are very thick.

Discussion of the I-V *and* EL-V *Characteristics*

CZ monomer is a constituent of the carbazole family. Some of them are well known, such as poly(*N*-vinyl carbazole) (PVK). This polymer has its HOMO located 5.7 eV below the vacuum level, whereas its band gap is 3.5 eV.[31] Assuming that the valence band of CZ locates also at about 5.5 eV and SnO_2 has a work function of 4.8 eV,[21] the hole energy barrier at the SnO_2/Cz interface is not too high (0.9 eV). In contrast, the energy barrier is much higher for electrons at the Al/CZ interface, because $F_{Al} = 4.25 \pm 0.15$ eV,[32] whereas the LUMO of the organic layer can be estimated to be around 2 eV, which induces a barrier height around 2.25 eV.

The PBrPDSe with a band gap of about (3.5 eV) has a *p*-type conductivity.[33] The forward current in organic diode devices is usually assumed to be mainly a hole current. This assumption agrees with studies on PVK material,[34] where carbazole groups are hole conducting and electron blocking materials. Otherwise, the diodes can be considered as metal/insulation/metal (MIM) structures with a current mainly controlled by holes injected at the SnO_2 contact. However, as shown in Table I, the turn-on voltage is low, which is a clear indication that substantial electron injection does occur. The PBrPDSe is nearly insulating and could behave as a hole-trapping layer. Owing to the trapping of holes, electron injection is made easier by improving the electron to hole current balance and enhancing the performance of the diodes.

Different models issued from inorganic structure are often used to roughly explain current such structures: Fowler–Nordheim tunneling emission,[35] Schottky thermionic emission.

We will discuss these two possibilities in light of experiments.[36]

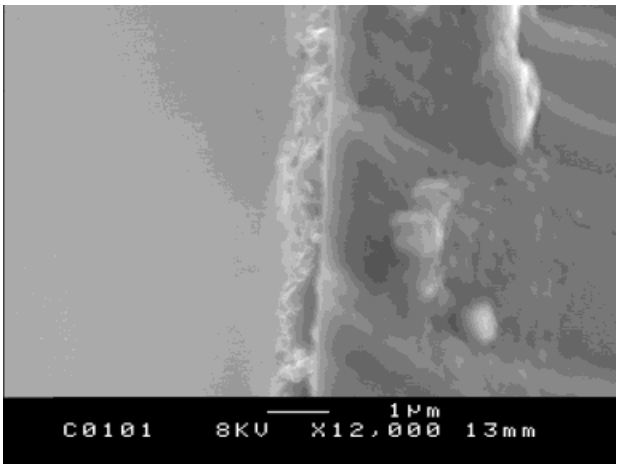

Figure 5 Cross section of a CZ film.

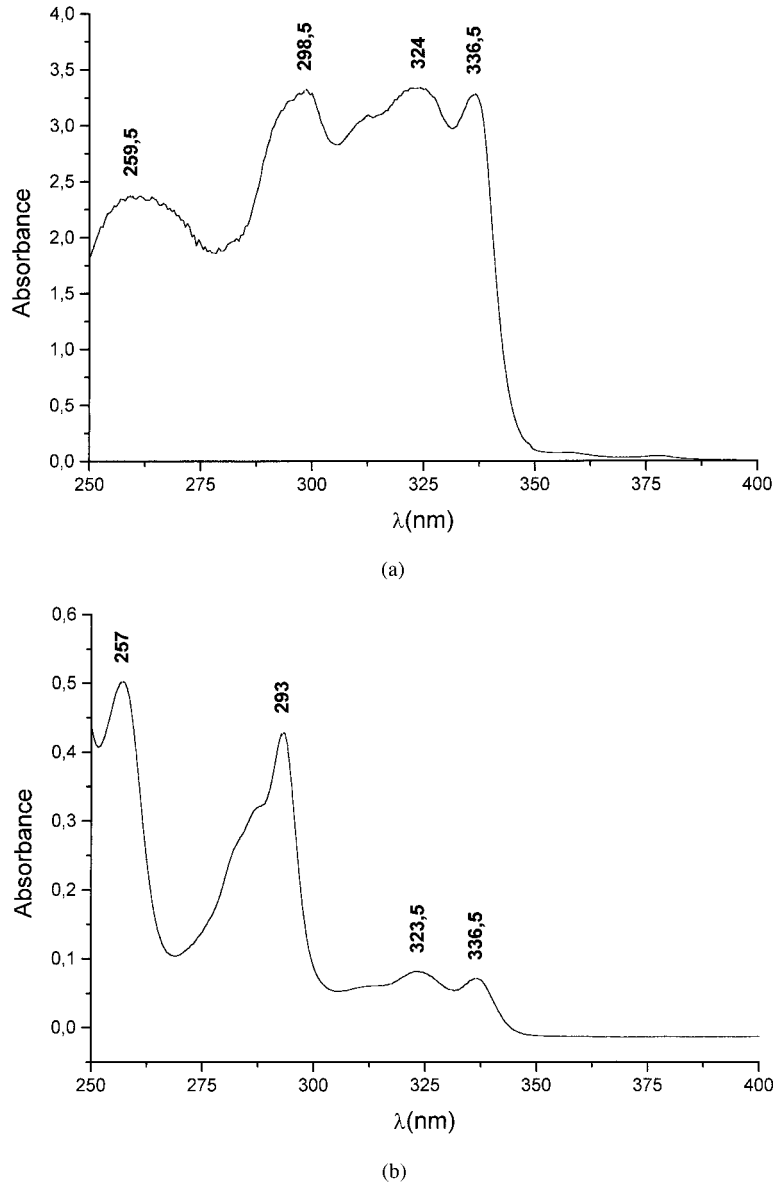

Figure 6 Transmission spectrum of CZ in solution in THF. (a) Reference powder; (b) thin film.

a. Fowler–Nordheim tunneling emission at high electric field is given by

$$J\alpha\frac{F^2}{d}\exp\left(-\frac{K}{F}\right)$$

where J is the current density, F is the electric field, ϕ is the interface barrier height, and

$$K=\frac{8\pi\sqrt{2m^*\phi^3}}{3qh}$$

where m^* is the effective mass of holes in the polymer.

The two films were insulated; for simplicity, in the case of double layers, we assume that the electric field is constant across the device and the effective mass is equal to the free electron mass.[37] From *I-V* characteristics shown Figure 8(b), the Fowler–Nordheim plot is drawn in Figure 9. Taking the slope, the K value is estimated and then the ϕ value is estimated; the same calculation was done for each sample in Table II. It can be seen that the estimated values vary between 0. 20

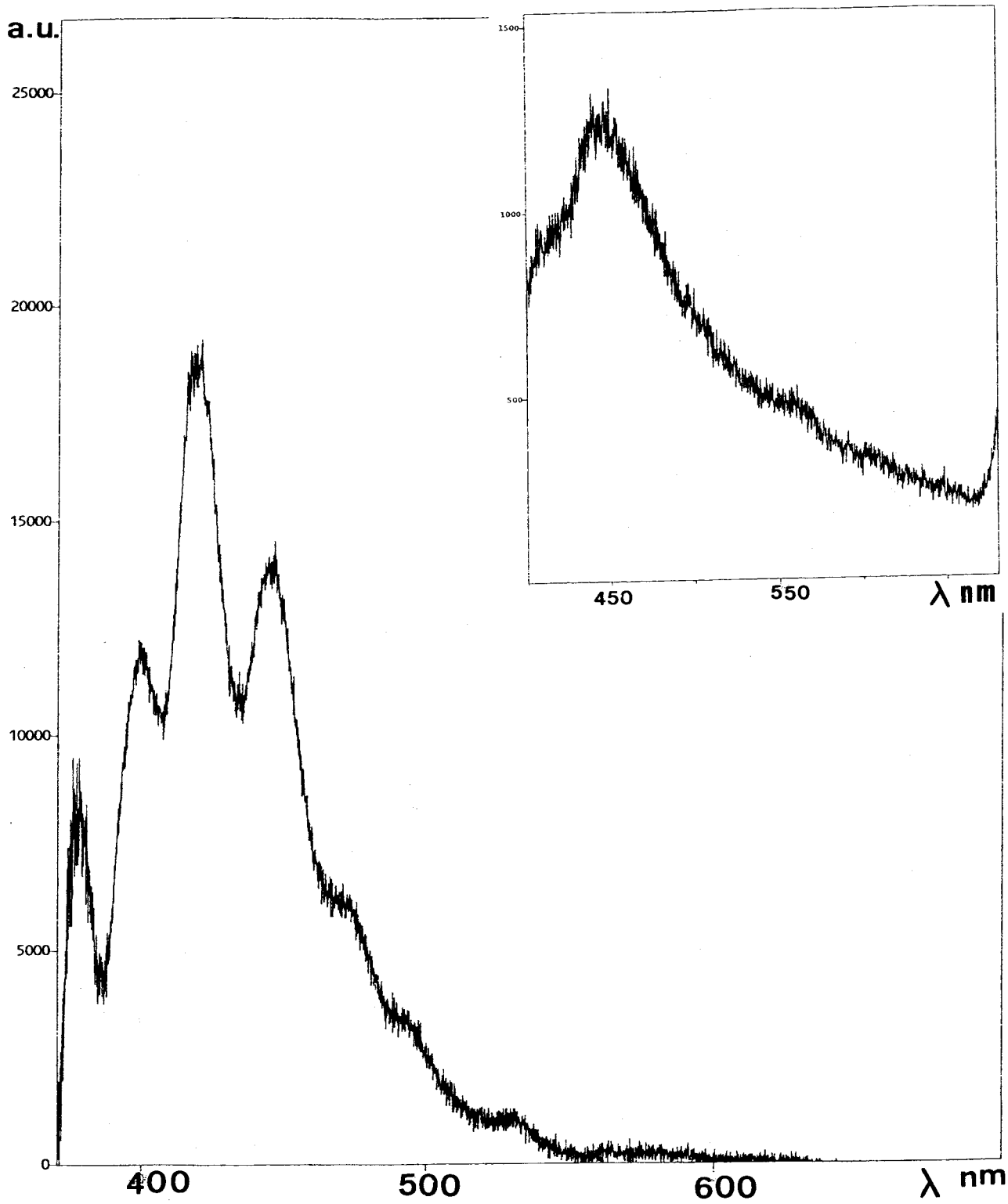

Figure 7 Luminescence spectrum of CZ powder. (Inset) Luminescence spectrum of PBrPDSe powder

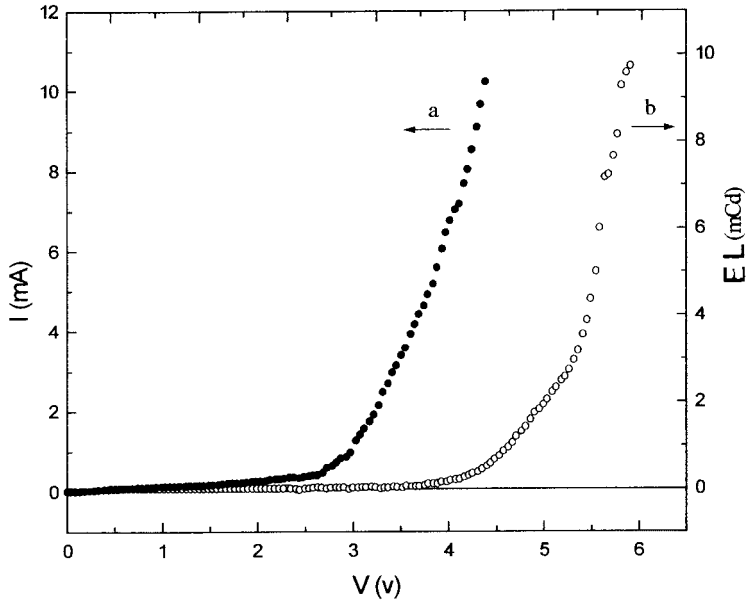

Figure 8 (*I-V*) and (*EL-V*) characteristics of a SnO_2/PBrPDSe/CZ/Al double-layer diode (CZ thickness: 200 nm).

and 0.40 eV in the case of the double-layer structure, whereas in the case of single layer, it varies between 0.3 and 0.73 eV.

b. Schottky Thermionic Emission

Nevertheless, almost every device studied showed a current increasing exponentially with bias over one to two orders of magnitude. In Figure 10, the *I-V* data from Figure 8(b) are potted semilogarithmically, because in the case of thermally activated Schottky diode mechanism, we have

$$J = J_0 \exp(qV/nkT)$$

where n is the ideality factor.

The barrier height ϕ_B can be deduced from:

$$J_0 = A^*T^2 \exp\left(\frac{-q\phi_B}{kT}\right)$$

with A^* as the Richardson constant.[36] The ideality factor can be deduced from $\Delta V/\Delta \ln J$, the inverse of slope ln J versus applied voltage since $n = q/kT(\Delta V/\Delta \ln J)$ in the exponentially increasing current domain. This ideality factor should vary between 1 (purely thermionic) and 2 (recombination in the space charge layer)[38]; however, as shown in Table II, it is often far higher, having no real physical meaning.

There is no clear connection between the organic layer thickness and the ideality factor value, which suggests that the bulk series resistance is not responsible for high n values (Table II).

Figure 11 demonstrates that the *I-V* characteristics for a typical double-layer sample show only a slight temperature dependence rather than the exponential dependence expected for thermionic

Table I Turn-On Voltages and Fields

ITO/CZ/Al Diodes		ITO/PBrPDSe/CZ/Al Diodes (thickness PBrPDSe 50 nm)		
CZ Thickness (nm)	Turn-On Voltage (V)	CZ Thickness (nm)	Turn-On Voltage (V)	Turn-On Field (Vm^{-1})
200	3.7	200	2.4	1.2×10^7
450	2.8	210	2.7	1.28×10^7
600	2.6	250	3	1.2×10^7
		350	3.3	0.95×10^7

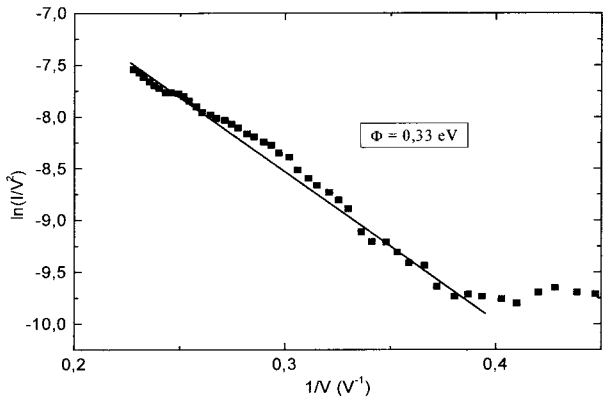

Figure 9 Fowler–Nordheim plot for SnO_2/PBrPDSe/CZ/Al double-layer diode (CZ thickness: 200 nm).

emission (as indicated by the solid line); it is almost temperature independent, suggesting tunneling.

Moreover, as shown in Table I, the turn-on effect is more field dependent than voltage dependent.

Such nearly temperature-independent and field-dependent behavior is usually associated with tunneling processes, which corroborates the Fowler–Nordheim theory, and therefore, we prefer an explanation for the high-voltage behavior which depends more on tunneling through a triangular barrier rather than Schottky barrier at a SnO_2/CZ interface.

A mechanism exists for carrier injection at the SnO_2 electrode, which has most of the features of tunneling through a triangular barrier (e.g., polymer thickness critical field dependence and only small temperature dependences), while showing the exponential voltage dependence suggestive of thermionic emission. This is thermionic field emission,[39] where carriers are thermally activated to give an increased tunneling probability through thinner and lower regions of the barrier. There is a smooth gradation between the pure thermionic emission and field emission.[40] In the present work, we are closer to field emission. Moreover, it should be noted that the voltage drop is distributed among the different layers and the conductivity of PBrPDSe, being a small part of the voltage drop, occurs in this layer and an important part of the critical field (Table I) should be localized in the PBrPDSe film.

The effect of the PBrPDSe layer can be interpreted as follows.

The instability of single-layer samples due to leakage current is an indication of pinholes in the polymer film. This is a problem due, at least partly, to the low-molecular weight of the carbazole monomer. The heterogeneity of the CZ films increases with its thickness, as shown in Table I and Figure 12. Moreover, Table I shows that even in the case of double-layer structure, when the CZ thickness overpasses 400 nm, the field-effect dependence of the turn on of the current disappears. Figure 12 shows that CZ crystal oriented perpendicularly to the plane of the substrate appears, which favors the upper electrode diffusion and decreases the real working polymer thickness.

In addition, in the case of single layer, the surface roughness of SnO_2 contributes also to the leakage phenomenon and CZ unhomogeneity. Therefore, the addition of the PBrPDSe layer serves as a buffer layer and hole-injection layer, while it eliminates the leakage problems. The PBrPDSe buffer layer first directly avoids (physically) the direct short circuit effect because of its high-coverage efficiency, and second, it modifies the surface roughness of SnO_2, which contributes to more homogeneous growth of CZ films. Moreover, as shown above, the measured barrier height ($0.20\ \text{eV} < \phi < 0.40\ \text{eV}$) is quite smaller than the one theoretically estimated (0.9 eV); it can be concluded that the PBrPDSe films not only introduce a mechanical insulating film between TCO and CZ films, but also decreases the barrier height at the interface, which allows better hole-injection efficiency. However, the discrepancy between experiment and theory can also be attributed to others' processes, which can also take place, such as space charge-limited current or field-dependent mobility, which could also be considered to rationalize the current voltage curves.

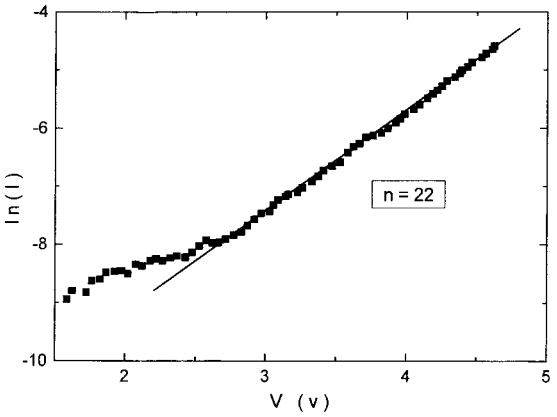

Figure 10 Semilogarithmic plots of (I-V) characteristics at large forward bias for sample of Figure 8(a).

Table II Ideality Factor *n* (Thermionic Model) and Barrier Height Φ (Fowler–Nordheim Model) for Different OLED

Structure SnO_2/PBrPDSe/CZ/Al								
Sample thickness (nm)	200	250	250	300	300	300	350	400
Ideality factor, *n*	17	13	25	30	15	20	27	18
Barrier height (eV)	0.27	0.25	0.35	0.30	0.20	0.40	0.26	0.35
Structure SnO_2/CZ/Al								
Sample thickness (nm)	200	300	400	500	600			
Ideality factor, *n*	12	23	18	21	27			
Barrier height (eV)	0.73	0.29	0.36	0.30	0.43			

In the present work, the turn-on voltages (and critical electrical field) are more or less one order of magnitude smaller than those usually found the this device family.[32] The same lowering effect was measured in other devices. Yang et al.[41] have shown that using a rough polyaniline (PANI) interfacial electrode between the TCO and polymer, the average local field is enhanced by approximately an order of magnitude, this enhanced local electric field being an intrinsic feature of the irregular rough surface of the self-assembled PANI-CSA network electrode. In the present work, no such anode exists because, if PBrPDSe exhibits as a filament-like structure, it is insulating. However, we have shown that the CZ-layer surface roughness is very high; therefore, the upper aluminum electrode is very rough, which could justify here also a field effect between under the electrode and these aluminum tips.

However, the secondary effect of these tips will be progressive aluminum diffusion, which justifies that, if there is no aging effect when they are not used, the diodes will still work 1 year after achievement, the lifetime of the diodes is quite short when they work.

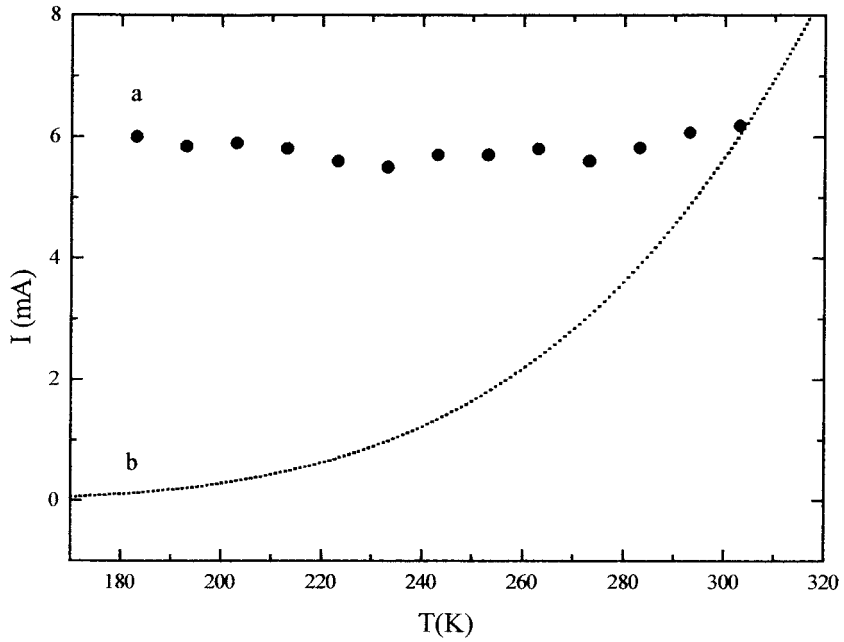

Figure 11 Temperature dependence of a SnO_2/PBrPDSe/CZ/Al double-layer diode (CZ thickness: 200 nm) operating at 3 V bias; for comparison, the solid line indicates the (*I-V*) characteristics of a 0.3 eV Schottky barrier device. (The barrier height is estimated from the *I-V* curves with $A^* = 120$ A/cm^2 K^2.)

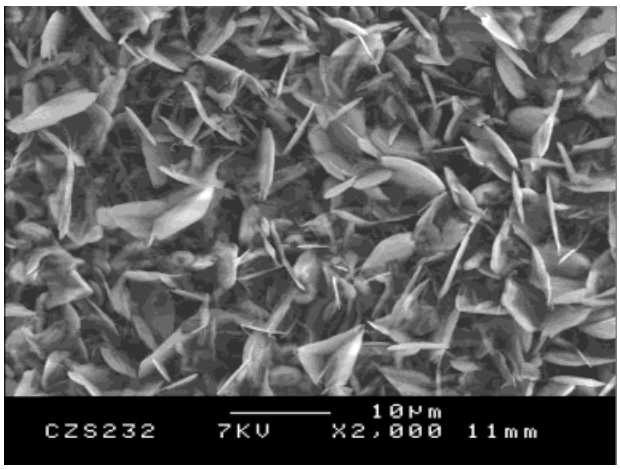

Figure 12 Micrograph of a thick CZ film (thickness: 600 nm).

That is to say, the diodes are chemically stable and after 1 year in room atmosphere their properties do not change, but when they are used, some localized heating related to the tip effect induces rapid degradation of the diode characteristics.

CONCLUSION

We have shown that the use of a homogeneous thin-polymer layer at the interface TCO/emissive film allows the improvement of the reproducibility and the living time of CZ-based OLED. The current mechanism is mainly based on tunneling injection of hole at the interface TCO/polymer. However, if analysis of the current-voltage characteristics shows that the dominant conduction mechanism can be thermally assisted tunneling, it cannot accurately explain the totality of the variation of the (*I-V*) properties, with temperature, for example,[42] and the models should be used only as a helpful tool to compare different structures.

The small atomic weight of CZ explains the difficulty of obtaining better results. However, because it is easy to deposit in thin-film form, the PBrPDSe effect can also be easily studied. More investigation should be pursued on the PBrPDSe films to obtain better information on the band structure of this promising polymer. This layer will be introduced in structure by using heavier molecular-weight samples such as PVK to obtain more stable structure.

This work was supported by the action ECOS-CONICYT No. 99-E05.

REFERENCES

1. Burroughes, J. H.; Bradly, D. D. C.; Brovn, A. R.; Morks, R. N.; Mackay, K.; Friend, R. H.; Burmond, P. L.; Holmes, A. B. Nature 1990, 374, 539.
2. Nguyen, T. P.; Destruel, P.; Molinié, P. in Organic and Polymer Based Light Emitting Diodes; Haria Singh Nalwa, Ed.; Handbook of Advanced Electronic and Phototonic Materials; Academic Press: San Diego, 2000.
3. Kusano, H.; Shiraishi, N.; Hosaka, S.; Kumura, I.; Kitagawa, M.; Ichino, K.; Kobayashi, H. Synth Met 1997, 91, 341.
4. Wang, G.; Yuan, C.; Wu, H.; Wei, Y. J Appl Phys 1995, 78, 2679.
5. Hu, B.; Yang, Z.; Karasz, F. E. J Appl Phys 1994, 76, 2419.
6. Yapi Abbe, S.; Bernede, J. C.; Del Valle, M. A.; Tregouet, Y.; Ragot, F.; Diaz, F. R.; Lefrant, S. Synth Met to appear.
7. Romero, D. B.; Schaer, M.; Leclerc, M.; Ades, D.; Siove, A.; Zuppiroli, L. Synth Met 1996, 80, 271.
8. Gelber, D. D.; Wang, Y. Z.; Fu, D. K.; Swager, J. M.; Eptain, A. J. J Chem Phys 1998, 108, 7842.
9. Marayan, K. S.; Murthy, G. L. Chem Phys Lett 1997, 276, 441.
10. Chao, C. I.; Chen, A.-A. Appl Phys Lett 1998, 73, 426.
11. Cho, H. N.; Kim, J. K.; Kim, D. Y.; Kim, C. Y. Macromol Symp 1997, 125, 133.
12. Meng, H.; Chen., Z. K.; Yu, W.-L.; Pei, J.; Liu, X.-L.; Lai, Y. H.; Huang, W. Synth Met 1999, 100, 297.
13. Han, E.; Do, L.; Yamamoto, N.; Fujihira, M. Mol Cryst Liq Cryst 1996, 280, 349.
14. De Leeuw, D. M.; Lous, E. J. Synth Met 1994, 65, 45.
15. Garnier., F.; Yassar, A.; Hajlaoui, R.; Horowitz, G.; Deloffre, F.; Servet, B.; Ries, S.; Alnot, P. J Am Chem Soc 1993, 115, 8716.
16. Tamada, M.; Omichi, H.; Okui, N. Thin Solid Films 1995, 268 18.
17. Ivanov, V. F.; Nekrasov, A. A.; Gribkova, O. L.; Vannikov, A. V. Synth Met 1996, 83, 249.
18. Blanchet, G. B.; Fincher, C. R., Jr. Adv Mater 1994, 6, 881.
19. Chen, B.; Liu, S. Jpn J Appl Phys 1998, 37, 1665.
20. Touihri, S.; Safoula, G.; Bernède, J. C.; Leny, R.; Alimi, K. Thin Solid Films 1997, 304, 16.
21. Gordon, R. G. Mat Res Soc Symp Proc 1996, 426, 419.
22. Osada, T.; Kugler, Th.; Bröms, P.; Salaneck, W. S. Synth Met 1998, 96, 77.
23. Kern, W.; Puotinen, D. A. RCA Rev 1970, Juin, 187.
24. Messoussi, R. Thèse d'état, Kénitra, Maroc, 1998.
25. Diaz, F. R.; Tagle, L. H.; Gargallo, L.; Radic, D.; Godoy, A. Polym Commun 1989, 30, 241.
26. Frigero, P. F.; Tagle, L. H.; Diaz, F. R. Polymer 1981, 22, 1571.
27. Godoy, A. Thesis, PUCC Santiago de Chile, Chile, 1993.

28. d'Almeida, K.; Bernède, J. C.; Godoy, A.; Diaz, F. R.; Mevellec, J. Y.; Molinié, P. Thin Solid Films to appear.
29. Beamson, G.; Briggs D. High Resolution XPS of Organic Polymers—The Data Scienta ESCA300 Database; Wiley: Chichester, 1992.
30. Bin Hu, Z.; Karasz F. E. Chem Phys 1998, 227, 263.
31. Zhang, Z. L.; Jiang, X. Y.; Xu, S. H.; Nagatomo, T.; Omoto, O. Synth Met 1997, 91, 131.
32. Parker, I. D. J Appl Phys 1994, 75, 1656.
33. Godoy, A.; Bernède, J. C.; J Chim Phys 1993, 90, 1491.
34. Lmimouni, K.; Legrand, C.; Chapaton, A. Synth Met 1998, 97, 151.
35. Simmons, J. G. J Appl Phys 1963, 34, 1793.
36. Sze, S. M. Physics of Semiconductor Devices, 2nd ed.; Wiley: New York, 1981; p 245.
37. Park, J. P.; Le, H. M.; Kim, G. T.; Park, H.; Kang, I. N.; Hwang, D. H.; Shim, H. K. Synth Met 1996, 79, 177.
38. Rodherick, E. H. Metal–Semiconductor Contacts; Clarendon: Oxford, 1978.
39. Mancini, A. M.; Dierini, P.; Valentini, A.; Vasanelli, R.; Quirini, A. Thin Solid Films 1985, 124, 85.
40. Jones, R.; Krier, A.; Davidson, K.; Schmit, J. P. N.; Zawadzka, J. Thin Solid Films 1999, 340, 221.
41. Yang, Y.; Westerweele, E.; Zhang, C.; Smith, P.; Heeger, A. Jpn J Appl Phys 1995, 77, 694.
42. Campbell, A. J.; Bradley, D. D. C. J Appl Phys 1999, 86, 5004.